JOURNAL OF GEOPHYSICAL RESEARCH, VOL. 91, NO. A2, PAGES 1283–1299, FEBRUARY 1, 1986

Plasma Waves Observed by the IRM and UKS Spacecraft During the AMPTE Solar Wind Lithium Releases: Overview

B. HÄUSLER,[1] L. J. WOOLLISCROFT,[2] R. R. ANDERSON,[3] D. A. GURNETT,[3] R. H. HOLZWORTH,[4] H. C. KOONS,[5] O. H. BAUER,[1] G. HAERENDEL,[1] R. A. TREUMANN,[1] P. J. CHRISTIANSEN,[6] A. G. DARBYSHIRE,[2] M. P. GOUGH,[6] S. R. JONES,[2] A. J. NORRIS,[6] H. LÜHR,[7] AND N. KLÖCKER[7]

The two September 1984 solar wind lithium releases produced a rich variety of plasma waves which have been measured in situ by the plasma wave instrumentation on board the Active Magnetospheric Particle Tracer Explorers (AMPTE) IRM and UKS spacecraft. Reflection of the natural galactic and terrestrial electromagnetic radiation from the dense Li plasma caused a cutoff in the high-frequency electric field intensities from which the temporal and spatial variation of the plasma density can be determined. Inside the diamagnetic cavity the electron plasma frequency and also temporarily the Li plasma frequency have been excited. The emission at the electron plasma frequency is near the thermal fluctuation level. In addition, weak low-frequency ion acoustic waves were observed. The boundary between the diamagnetic cavity and the external magnetic field was found to be surprisingly stable and contained extremely low levels of wave activity. In the transition region from the diamagnetic cavity to the solar wind, high wave activity at the medium and very low frequencies propagating mainly in the ion acoustic and electrostatic cyclotron harmonic modes was encountered. No wave magnetic fields were detected in this region. The upstream edge of the transition region was characterized by a steep decay in magnetic field strength and density and by a sudden increase in the quasi-static electric field. At this time the ELF/MF rms wave amplitude explosively increased to a value of 50 mV/m and remained at an enhanced level for more than 1 min. The spectrum of this wave activity is similar to the electrostatic noise observed in collisionless shocks. Data from UKS indicate that during the releases, UKS was in the magnetic transition zone. The wave activity at UKS was distinctly different from that encountered by IRM. The intense emission at the electrostatic shocklike transition was weaker than that on IRM and for the second release appeared at a different time. This can be related to the different positions of the two spacecraft with respect to the interaction regions. Despite the high wave intensities the estimated wave energy densities are, however, too low by orders of magnitude to drive significant magnetic field diffusion during the in situ observation times. Some differences in the wave excitations for the two releases can be traced back to the different solar wind conditions.

1. INTRODUCTION

As part of the Active Magnetospheric Particle Tracer Explorers (AMPTE) program, two Li^+ ion clouds were generated in the solar wind on September 11 (0725 UT) and September 20 (0956 UT), 1984. Three satellites participated in these experiments: the German AMPTE IRM spacecraft [*Häusler et al.*, 1985*a*], the British AMPTE UKS spacecraft [*Ward et al.*, 1985], and the U.S. AMPTE CCE spacecraft [*Dassoulas et al.*, 1985]. The overall scientific concept and the AMPTE mission aspects are described by *Acuña et al.* [1985].

During each release a total of $N_0 \approx 10^{25}$ Li atoms were injected into the solar wind from two symmetrically separated canisters. In situ plasma diagnostic measurements were performed by the IRM and UKS. In both cases the UKS was positioned approximately 35 km away upstream of the IRM. The CCE was located deep inside the magnetosphere in order to detect Li^+ ions transported from the solar wind into the magnetosphere. A detailed description of the technical aspects of the Li experiment is contained in the work by *Haerendel et al.* [1985]. The physics of the releases and the interaction of the Li cloud and the solar wind are described by G. Haerendel et al. (unpublished manuscript, 1985) and G. Haerendel (unpublished manuscript, 1985). In summary, the two Li clouds evaporated symmetrically from positions about 2 km from the IRM spacecraft with an expansion velocity of about $V_{exp} =$ 3–4 km/s. The clouds reached the IRM spacecraft about 0.5 s after release and merged into a single radially expanding cloud initially centered on the IRM. As the clouds expanded, photoionization by solar ultraviolet radiation produced a dense Li plasma with average ionization time of about $\tau_i \approx 1$ hour. The plasma density in the center of the cloud is expected to vary as $n(t) = 3N_0/4\pi V_{exp}{}^3 \tau_i t^2$ for times $t \ll \tau_i$. The interaction of the dense Li plasma with the solar wind is shown schematically in Figure 1. Initially, pressure balance between the plasma and the interplanetary magnetic field leads to the formation of a diamagnetic cavity around the IRM spacecraft. Momentum exchange between the lithium plasma and the solar wind results in a pileup of the magnetic field upstream of the cavity (G. Haerendel, unpublished manuscript, 1985). We will call the region between the diamagnetic cloud and the recovery of the magnetic field to its solar wind level the transition region. The transition region itself consists of three subregions: the current layer at the boundary of the cavity, characterized by the steep increase of the magnitude of the magnetic field $B = |\mathbf{B}|$; the magnetic compression zone; and the shocklike transition to the solar wind, indicated by the magnetic field recovery. Upstream of the transition region the solar wind is distorted by the presence of newly created dilute Li plasma. This region is called the upstream region. We will refer to these regions in the text of this paper.

Actually, the IRM was near the center of the cloud only for the time when the interaction was dominated by the dense Li^+ ion plasma. When the momentum given to the cloud by the

[1]Institut für extraterrestrische Physik, Max-Planck-Institut für Physik und Astrophysik, Garching, Federal Republic of Germany.
[2]Physics Department, University of Sheffield, Sheffield, United Kingdom.
[3]Department of Physics and Astronomy, University of Iowa, Iowa City.
[4]Geophysics Program, University of Washington, Seattle.
[5]The Aerospace Corporation, Los Angeles, California.
[6]University of Sussex, Falmers, Brighton, Sussex, United Kingdom.
[7]Institut für Geophysik und Meteorologie, Technische Universität Braunschweig, Braunschweig, Federal Republic of Germany.

Paper number 5A8627.
0148-0227/86/005A-8627$05.00

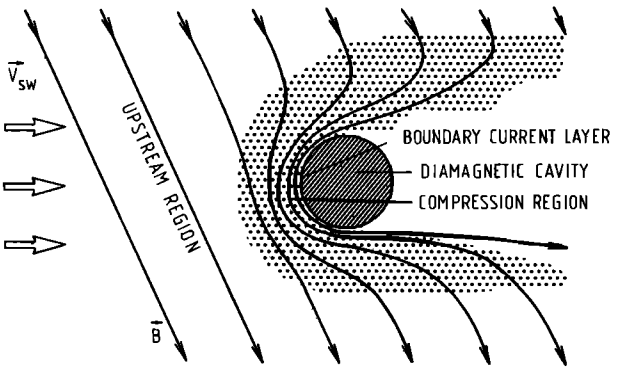

Fig. 1. Schematic representation of the interaction between the dense Li plasma cloud and the magnetized solar wind. The dotted region is the transition region between the cloud and the solar wind.

impact of the solar wind increased, the entire plasma cloud started moving approximately downstream, being carried away by the solar wind across the position of the IRM. Thus the IRM can be considered as moving out of the center of the cavity in an upstream direction, thereby crossing the outer parts of the cavity, its boundary, and the region of transition to the solar wind.

A visualization of the variation of B at the position of the IRM spacecraft for both releases is given in the top parts of Figures 2*a* and 2*b*. The sudden decrease of B to a low value near zero indicates the entrance of the IRM into the diamagnetic cavity. At the steep increase of the magnetic field the spacecraft crosses the boundary current layer and enters the transition region. It passes through the magnetic field compression zone and the shocklike transition to the solar wind and subsequently enters the upstream region. These general features are common for both releases. Remarkable differences in the releases are in the duration of the cavities and in the length and structure of the transition regions. The reasons for these differences have been discussed by G. Haerendel (unpublished manuscript, 1985).

The main scientific goal of the in situ measurements performed with the wave experiment was the investigation of the microscopic interaction of the artificial cold plasma with the streaming solar wind plasma. It is the first time that measurements of this kind have been made. Important subjects of this investigation are the wave activity excited (1) inside a diagmagnetic cavity, (2) in the transition region between the artificial and natural plasmas, and (3) in the upstream region.

In case 1 the unmagnetized dense expanding cold plasma cloud dominates. Only certain plasma modes (ion acoustic and Langmuir waves) are expected to be excited in the cavity. In case 2, strong gradients in plasma density and magnetic field arise owing to the interaction of the solar wind with the magnetized Li^+ plasma. Enhanced wave activity of a large variety of plasma modes is expected (current- and gradient-driven waves as well as beam instabilities in magnetized plasmas). These waves may play a role in the momentum exchange between the solar wind and the cloud plasma and possibly in the diffusive processes which control the dynamics of the interaction. For a discussion of various questions related to the behavior of artificial plasma clouds injected into the magnetosphere, see *Scholer* [1970] and *Pilipp* [1971].

Case 3 is characterized by a solution where the Li^+ plasma is diluted below solar wind density and where the single Li^+ ions are accelerated in the solar wind electric field, thereby forming an ion beam. The plasma modes to be expected now include beam modes and streaming instabilities. In addition, anisotropic heating of the electrons should lead to the excitation of electrostatic electron cyclotron waves and whistler mode waves.

A detailed technical description of the IRM plasma wave instrument has been given by *Häusler et al.* [1985*b*]. In brief, this instrument uses a long dipole antenna (47 m tip to tip) for the electric field measurements and two search coil antennas for the magnetic field measurements. The data presented here cover a frequency range from quasi-static (dc) to ~5 MHz. The time resolution was 1 s. Analog data transmissions covering a bandwidth of 10 kHz are also available. For both releases one magnetic antenna operating in the frequency range from 28 kHz to 1.5 MHz was connected to one of the stepped frequency receivers. During the second Li release one frequency analyzer on the IRM spacecraft was also connected to a magnetic antenna covering from 275 Hz to 2.525 kHz. Short time scale wave phenomena were recorded on IRM by a burst memory with time resolution of 32 ms. The spacecraft spin period was about 4 s.

The UKS wave experiment uses an electric dipole antenna consisting of carbon-coated spheres containing preamplifiers at the ends of two booms in the spin plane of the spacecraft (7 m tip to tip). *Darbyshire et al.* [1985] describe the instrument in more detail.

The present paper gives an overview of the wave measurements obtained with the two spacecraft IRM and UKS in the diamagnetic cavity, the transition region, and the upstream region. Special aspects of the wave observation and excitation are the subject of three other papers: R. R. Anderson et al. (unpublished manuscript, 1985) consider the determination of the plasma density from the measurement of the electron plasma frequency during the releases; *Gurnett et al.* [this issue] present an analysis of the intense emission in the shocklike transition region in terms of a beam instability; H. C. Koons et al. (unpublished manuscript, 1985) investigate the nature of the electron cyclotron emissions in the upstream region.

The structure of this paper is as follows. In section 2 we give the solar wind conditions during the two releases. Section 3 presents the observations. We have chosen to order the data according to the different wave bands while discussing the emissions in the three physical regions of the Li plasma–solar wind interaction. In section 4 this order is changed. Here we discuss the wave excitations in the diamagnetic cavity, the transition region, and the upstream region from a more physical point of view. Section 5 summarizes the results of the investigation.

2. Solar Wind Conditions and IRM/UKS Positions

Table 1 summarizes the solar wind conditions for the two Li^+ ion releases. A more detailed description of these conditions can be found in papers by *Haerendel et al.* [1985], *Paschmann et al.* [this issue], and *Lühr et al.* [this issue].

During the first release the solar wind velocity was very high (700 km/s). The direction of the magnetic field was approximately parallel to the direction of the solar wind flow. The release took place during a period of the presence of upstream ions reflected at the bow shock [*Paschmann et al.*, this issue]. During the second release the interplanetary conditions were quite different. The magnetic field direction was approximately perpendicular to the flow velocity. Therefore this release was closer to ideal conditions. The orbit positions of the IRM and UKS spacecraft for the two releases (Septem-

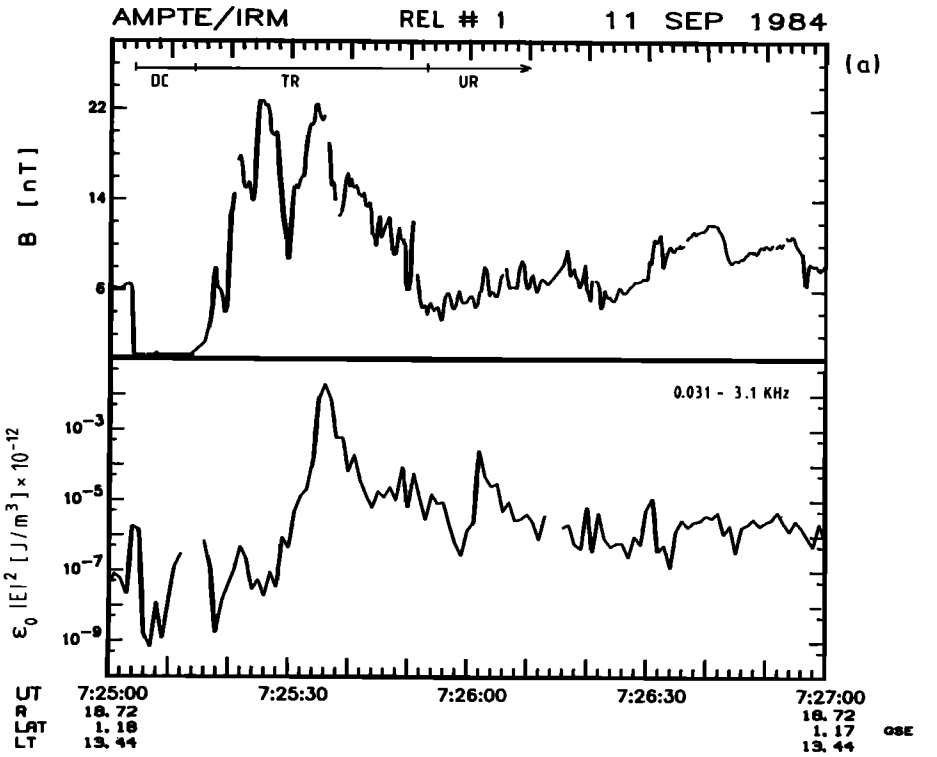

Fig. 2*a*

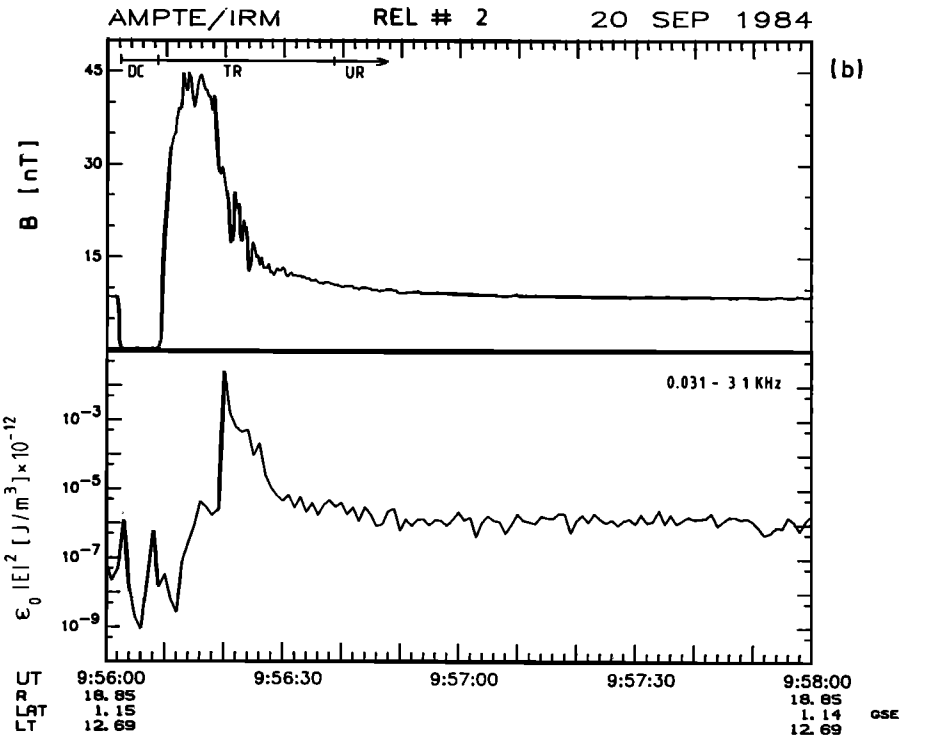

Fig. 2*b*

Fig. 2. Magnitude B of magnetic field (top panels) and power density (bottom panels) of the low-frequency waves (0.031–3.1 kHz) as measured by the IRM spacecraft for (*a*) release 1 and (*b*) release 2. The horizontal lines in the top panels indicate when IRM is in the diamagnetic cavity (DC), the transition region (TR), and the upstream region (UR). The transition region consists of three subregions: the boundary current layer where the magnetic field increases steeply from near zero to a value above the undisturbed solar wind value, the compression region, and the region of shocklike decay to the solar wind. The wave power density shows little activity in the diamagnetic cavity and the boundary current layer. Intense emission coincides with the shocklike transition region. Enhanced activity is found in the upstream region.

TABLE 1. Interplanetary Conditions

	Release 1	Release 2
n, cm^{-3}	1–4	4–10
V_{sw}, km/s	680	460
φ_V, deg*	171.5	175.0
θ_V, deg*	+3	+4
B, nT	6	8.5
φ_B, deg*	4.0	120.0
θ_B, deg*	−10	+15

*Angles in GSE coordinates.

ber 11, 1984, 0725 UT and September 20, 1984, 0956 UT) are given in a paper by G. Haerendel (unpublished manuscript, 1985).

UKS was approximately 35 km away from IRM for both releases. UKS was just inside the diamagnetic cavity for release 1 and just outside the cavity for release 2. In both cases the UKS was upstream of the IRM.

3. DATA PRESENTATION

In this section we give an overview of the data obtained from the different receivers of the plasma wave instrument. More detailed data and discussions of the excitation mechanisms are left for separate investigations presented in other papers [*Gurnett et al.*, this issue; R. R. Anderson et al., unpublished manuscript, 1985; H. C. Koons et al., unpublished manuscript, 1985].

3.1. *Quasi-Static Electric Field and Wideband Observations Aboard IRM*

Quasi-static electric field. In the dilute solar wind the measurements of the quasi-static electric field are not valid [*Häusler et al.*, 1985*b*]. The quasi-static electric field signal is entirely determined by the cloud of photoelectrons surrounding the spacecraft. The photopulse is much higher than the 4-s spin-modulated signal caused by the $\mathbf{V} \wedge \mathbf{B}$ field in the solar wind. However, during the releases when the IRM spacecraft was embedded in the dense Li plasma clouds, the conditions were similar to those of the ionosphere, and the photopulse developed into a small distortion of the spin signal, thus allowing a measurement of the quasi-static electric field. The resolution was 104 μV/m for release 1 and 26 μV/m for release 2.

Figure 3 shows the variations of the potential difference V_{Diff} between the two antennas (top panels of each pair) during release 2 together with fast time-resolved spectrograms of the wave electric fields (bottom panels of each pair) between 31 Hz and 178 kHz. Each panel of the figure contains 10 s of observations so that the V_{Diff} observations can be directly related to the wave spectrograms. The latter observations will be discussed separately in section 3.4.

The cloud encounter was clearly indicated in V_{Diff} by a drastic decrease in the quasi-static electric field signal at 0956:01.7 UT. This behavior is expected because of the much higher electron density in the ion cloud. The return of the magnetic field is marked by a gradual increase in the quasi-static electric field signal.

The potential difference V_{Diff} has a quasi-sinusoidal variation in the cloud. The field amplitude as determined from V_{Diff} is surprisingly large, of the order of $\sim \pm 2$ mV/m. However, polarization fields as high as this value are not expected to be present in the unmagnetized plasma of the Li cloud (see also section 4.2). So the nature of quasi-static electric field signals will have to be investigated further to consider possible sources of error in the field measurement. At 0956:18.7 UT the V_{Diff} signal suddenly increases and saturates for about 1 s, until it finally assumes its approximate solar wind form. This occurs coincidently in time with the abrupt decrease in number density and the onset of the intense shocklike electrostatic noise.

Wideband observations. Figure 4 shows high-resolution wideband spectral observations during release 2. The second and fourth panels from the top cover the entire range of 0–10 kHz, and the first and third panels resolve the first 0–1 kHz. No clear signature at the onset of the release, which was at 0956:1.7 UT, can be detected in the 0- to 1-kHz channel, but a spiky broadband emission covering the higher-frequency range is seen in the 0- to 10-kHz channel. The wave activity in the diamagnetic cavity is reduced. From 2 to 4 s after release, a narrow-band wave emission appears between 200 and 250 Hz. Two diffuse spin-modulated spots also occur about 4–7 s after release below 3 kHz. The Li plasma frequency at this time was at 3 kHz and decreased to 2 kHz 7 s after release. These emissions are possibly related to an excitation in the vicinity of the Li^+ ion plasma frequency.

The encounter of the transition region is marked by the onset of more intense low-frequency noise (as also seen in the burst memory (Figure 3) and peak data (Figure 5)). This noise is most intense below 300 Hz but intensifies at higher frequencies when the center of the transition zone is approached.

On the background of the noise there appear a number of spiky intense broadband emissions seen up to frequencies of about 10 kHz. The duration of these spikes is only a fraction of a second. They are separated by gaps containing no high-frequency emissions.

The modulation frequency of the spiky emissions in the transition region decreases with time from about 11 Hz to about 5 Hz just before the transition into the solar wind. The former frequency is near the lower hybrid frequency of a Li-dominated plasma in a 40-nT magnetic field, whereas the latter is about the lower hybrid frequency of the solar wind. In the transition region, lower hybrid wave activity may thus play some role. Further evidence will be given below (see section 4.3).

In the wideband data the onset of the shocklike region intense plasma emission at 0956:19 UT [*Gurnett et al.*, this issue] is recognized as a slight intensification and widening of the low-frequency noise up to frequencies around 800 Hz; in the higher frequencies a diffuse spike appears, followed by a gradual decay in intensity which at later times is periodically modulated. Comparison with the quasi-static electric field shows that the diffuse intense emission is related to the shocklike transition region from cloud to the solar wind, marked by the sudden increase in the quasi-static electric field intensity (Figure 3).

After 0957:00 UT the IRM is in the upstream region. Here one observes diffuse electron cyclotron harmonics. The first four harmonics are visible at frequencies between harmonics of the electron cyclotron frequency f_{ce}. These emissions are of a general type known as electron cyclotron waves and occur near $f \approx (n + \frac{1}{2}) f_{ce}$, where $n = 1, 2, 3, 4, \cdots$ (H. C. Koons et al., unpublished manuscript, 1985).

3.2. *High-Frequency Waves*

The dynamical spectra of the high-frequency magnetic (HF-B) and electric (HF-E) emissions obtained every 2 s are shown in Figure 5 for release 2. The frequency scale is given in Table 2. (Note that the HF-B instrument was commanded

into a mode which covers the frequency range from 28 kHz to 770 kHz. This is only half of the full range of the picture. We have therefore plotted each second sweep of the spectrum in the space above the dashed line. This procedure leads to a doubling of the dynamical spectra.)

The high-frequency magnetic wave field does not show any response to the release. The various stationary signals are spacecraft interference lines. In the electric high-frequency field one observes a spin- and direction-modulated signal whose central frequency is around 300 kHz. Weak emissions at higher frequencies are also recorded. The structured emission is of terrestrial origin (terrestrial kilometric radiation (TKR) [*Gurnett* 1974, 1975]), while the weak isotropic high-frequency emission is consistent with the galactic radio noise (GRN) spectrum [*Brown*, 1973]. An interference line shows up in the highest frequencies.

The onset of the release is marked by a sudden dropout of the intensity of both GRN and TKR up to frequencies of about 4 MHz, which is due to the reflection of the radiation by the dense Li plasma cloud. The gradual reappearance of the radiation successively from higher to lower frequencies can be interpreted as the decrease of the plasma density during expansion of the cloud. Both this recovery and the excitation of the electron plasma frequency in the cloud, which could be detected during specific time intervals, permit a determination of the electron density (R. R. Anderson et al., unpublished manuscript, 1985) in the cloud. (The variation of the density obtained by this method is shown in Figure 10).

In the bottom panel of Figure 5 we show the peak spectrograms of the electric wave field between 31 Hz and 178 kHz, i.e., in the extremely low frequency/medium-frequency range [*Häusler et al.*, 1985*b*]. The low-frequency channels of the HF-*E* instrument and the high-frequency channels of the ELF/MF instrument overlap. The TKR is identified in the VLF/MF receiver as the two weak high-frequency emission bands above 56 kHz. The band at 178 kHz is the auroral kilometric radiation (AKR), while the band at 56 kHz is the escaping terrestrial continuum. Again, the emission-free region starting at the release indicates the reflection of the external radiation at the cloud. The recovery of the radiation after some seconds, starting at higher frequencies and progressing to lower frequencies, also here indicates the decrease of the plasma density in the Li plasma cloud due to its expansion. The subsequent intensification of the TKR in the high-frequency electric waves and the upper channels of the VLF/MF instrument after 0956:20 UT when the satellite is in the upstream region is a natural effect and is probably not related to the release.

The electron plasma frequency in the cloud region is marked by the dotlike emission around 100–300 kHz in the high-frequency electric spectra after 0956 UT and appears in the VLF/MF peak spectra around 17–31 kHz after about 0957 UT. This latter emission is at the solar wind plasma frequency.

3.3. *Medium-Frequency and Very Low Frequency Waves*

Figures 6*a* and 6*b* show spectrograms of the emissions recorded in the 31-Hz to 178-kHz band for both releases using the ELF/MF spectrum analyzer and the ELF/MF stepped frequency receiver (SFR) on board the IRM. The frequency scales are given in Tables 3 and 4. Two types of spectrograms are shown. The peak spectrogram gives the peak intensity measured during the 1-s integration time of the plasma wave instrument. The average spectrogram shows the 1-s averages of the wave intensity.

In the ELF/MF peaks and averages prior to release 1 (Figure 6*a*) one observes a well-defined emission at the solar wind electron plasma frequency which was around 9–18 kHz, corresponding to a solar wind density of 1.3–4.0 cm^{-3}. This emission is also seen in SFR 3. During the release the plasma frequency shifts to high frequencies outside the range of the ELF/MF and SFR instruments and is found in the HF electric wave band (R. R. Anderson et al., unpublished manuscript, 1985). This shift is caused by the steep increase of the plasma density inside the Li plasma cloud. The dropout of all wave activity at 0725:03 UT in the ELF/MF, SFR, and high-frequency electric field occurs almost precisely at the encounter of the Li plasma cloud. After 0725:30 UT the plasma frequency comes down in frequency again from the HF into the ELF/MF range when the IRM leaves the transition region and enters the upstream region. For a few minutes after release, the density seems to remain slightly enhanced in comparison with the prerelease solar wind ($\approx$4–10 cm^{-3}).

The most remarkable observation in this frequency range is, however, the sudden onset of intense wave activity below 3 kHz at about 0725:35 UT in the outer part of the transition region coincident with the shocklike region [*Gurnett et al.*, this issue] near the boundary between the solar wind and the Li plasma cloud. This emission has a highly dynamical character. Its most impulsive part lasts for about 4 s, but the total duration of the intense emission is about 12 s.

Enhanced ELF/MF plasma wave activity is observed subsequently in the upstream region for about 5 min, as seen in the peaks and averages and also in the SFR data. In addition, the upper cutoff frequency of the emissions decreases gradually with time. After the impulsive intense emission event the SFR also indicates the presence of a harmonic structure in the broadband emissions. The harmonic emission is of diffuse nature and has a bandwidth of roughly $\Delta f \approx 100$ Hz. It has been tentatively interpreted as electron cyclotron waves excited either by the anisotropically heated electron component of the newly ionized lithium gas or directly by the Li^+ ion beam (H. C. Koons et al., unpublished manuscript, 1985).

The measurements obtained during release 2 resemble those of release 1 except for their shorter total duration and greater quietness. Figure 6*b* shows both the ELF/MF peak and average data, the SFR spectrograms, and the SFR magnetic wave field measurements. The top panel is identical with the peak spectrogram of Figure 5. The magnetic wave fields were obtained from a SFR (0.2–2.5 kHz) which was connected to the magnetic antenna. The ELF/MF measurements show the weak stable low-frequency emissions of the quiet solar wind prior to the release.

The release encounter is marked by a short intense broadband pulse, followed by a period of very low wave intensities inside the diamagnetic cavity. Some impulsive emissions are seen in the diamagnetic cavity.

The transition from the cavity to the transition region is marked by an intensification of the low-frequency emissions. Moreover, the plasma wave intensity and the upper frequency cutoff gradually increase as the magnetic field increases in the boundary current layer toward the compression region. When the IRM approaches the region of shocklike transition to the solar wind, an intense emission is encountered. The increase in intensity is much steeper than that for the intense emission of release 1. The SFR also records the very intense broadband burst. The enhanced intensity is also reflected by the increase in the automatic gain control (AGC) of the wideband receiver

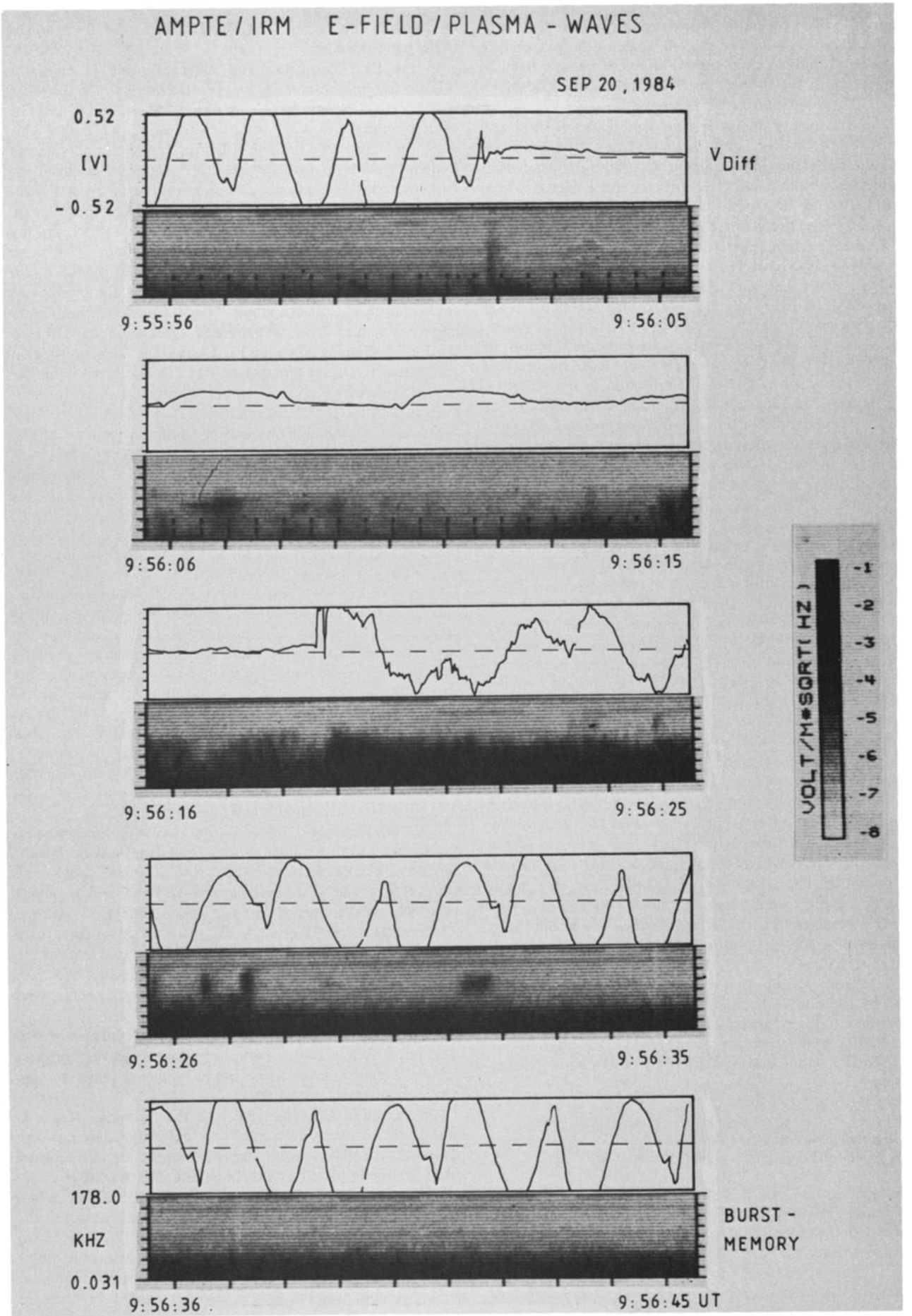
AMPTE / IRM E-FIELD / PLASMA - WAVES
SEP 20, 1984
0.52
[V]
- 0.52
V Diff
9:55:56
9:56:05
9:56:06
9:56:15
9:56:16
9:56:25
9:56:26
9:56:35
178.0
KHZ
0.031
9:56:36
9:56:45 UT
BURST - MEMORY
VOLT/M*SQRT(HZ)
-1
-2
-3
-4
-5
-6
-7
-8

(bottom panel of Figure 6b). This burst of intense emission is, however, very short. It lasts for about 1 s, as will be shown in sections 3.4 and 3.5. After this time the wave intensity decreases gradually but remains enhanced for several minutes after release throughout the upstream region. It should be noted that around 0957 UT the upper frequency cutoff of the spectrum is shifted up to a frequency of 3–4 kHz. This widening of the spectrum is seen very well in the SFR recordings. Moreover, a narrow but diffuse emission between 178 and 311 Hz is observed. In the magnetic wave field measurements above 200 Hz there was no indication of a magnetic component of wave emission throughout release 2. As for release 1 there are again some indications of the presence of diffuse electron cyclotron harmonics (H. C. Koons et al., unpublished manuscript, 1985). The diffuse emission may tentatively be identified with the lowest-frequency $(3/2)f_{ce}$ harmonic emission [*Ashour-Abdalla and Kennel*, 1975].

3.4. *Fast Time Resolution Burst Observations*

The bottom panels (spectrograms) of Figure 3 show 1 min of the burst memory data obtained with the ELF/MF receiver of the plasma wave instrument during release 2. Each panel contains 10 s of observations with 32-ms time resolution. The first spectrogram from the top shows the quiet solar wind natural low-frequency noise and the spin-modulated spacecraft noise produced by the solar panels. At 0956:1.7 UT a pulse of 0.2 s duration extending up to frequencies of ~100 kHz marks the passage of the lithium cloud from one of the canisters over IRM; a second pulse 0.3 s later indicates passage of the second cloud produced by the second canister. These pulses can be distinguished from the solar array spikes. Both passages together produce an emission with a duration of 0.7 s in the lowest (31 Hz) channel. Afterward, inside the diamagnetic cavity the noise is attenuated for about 3 s. Only some patchy emissions with maximum intensity at 1 kHz and a cutoff at 3 kHz are detected inside the diamagnetic cavity. This observation is consistent with the wideband data. At the time of these emissions the cavity is just 5 s old. The patchy emissions seem to be near the Li^+ ion plasma frequency, which at this time was $f_{Li} \approx 2.7$ kHz.

Both the bandwidth and the intensity of the low-frequency waves above 31 Hz are reduced between 0956:09 and 0956:12 UT when the IRM satellite traverses the boundary current layer of the diamagnetic cavity and enters the transition region. In the magnetic field compression region of the transition region the low-frequency noise intensifies gradually while the spectrum widens in frequency toward higher frequencies, until at 0956:18.7 UT, intense emission related to the shocklike region sets in. Its intensity is highest at 200–300 Hz, lasting for only 0.2 s. The emission is hence very impulsive. Thereafter, the intensity and maximum frequency rapidly decrease. About 5 s later the emission has merged into a still enhanced wave activity. Some impulsive structure can be observed in the later phase of the intense emission burst after 0956:20 UT, but after 0956:25 UT the emission has undergone a smooth transition to the postrelease enhanced emission level in the upstream region.

Similar observations have been obtained during release 1. During release 1 the solar wind electron plasma frequency was more intense than during release 2. Also, the intense emission of the shocklike region was distributed over a longer time and was much more diffuse. Here, right after the intense emission the electron plasma frequency indicates that the electron density has returned approximately to its prerelease solar wind level (R. R. Anderson et al., unpublished manuscript, 1985).

3.5. *Wave Power and Spectra*

The wave energy density integrated over a frequency range from 30 Hz to 3 kHz is shown in the bottom panels of Figure 2 for the two releases. There are remarkable differences between release 1 (Figure 2a) and release 2 (Figure 2b). The electric and magnetic field intensities for release 2 were less disturbed than those for release 1. We therefore concentrate on release 2 and subsequently compare the measurements from release 2 with those from release 1.

The wave energy density in the solar wind was about 3×10^{-20} J/m^3 prior to both releases. Figure 2b shows that the wave energy density decreases by roughly 2 orders of magnitude inside the diamagnetic cavity and stays low until the magnetic field rises to its maximum compression at 0956:12 UT. Superimposed are two short intensifications at 0956:02 UT and 0956:08 UT. The first can be related to the encounter of the cavity and the IRM spacecraft; the second is identified as the contribution of the spiky emission inside the diamagnetic cavity below 3 kHz mentioned in section 3.4 and seen in Figure 3. So, inside the diamagnetic cavity the wave energy density above 31 Hz is extremely low. However, the most remarkable observation is that the wave energy density is very low in the current layer between the diamagnetic cavity and the transition region.

In the magnetic field compression region the energy density rises steeply by 3 orders of magnitude over a time of only 4 s, indicating that there is intense wave turbulence below 3 kHz. However, in the shocklike region it increases explosively by an additional 4 orders of magnitude, reaching a value of about 6×10^{-13} J/m^3, corresponding to a rms electric wave amplitude of $E_{rms} = 50$ mV/m. This intense emission lasts for only 1 s. The wave energy density afterward decreases rapidly toward the end of the transition region to a level 2 orders of magnitude above that of the solar wind, which only slowly decays further throughout the upstream region.

The intense shocklike emission is the most interesting event observed. Its origin has been attributed to an ion beam-plasma interaction as discussed by *Gurnett et al.* [this issue]. One would expect that the high noise level would contribute

Fig. 3. (Opposite) (Top panels: graphs) Potential difference V_{Diff} for release 2 measured along the antenna boom after $t_0 = 0955:55.59$ UT. The time resolution is 32 ms. Each panel contains 10 s of observations. The sensitivity was $-0.52\ V \le V_{Diff} \le 0.52\ V$. The initial large-amplitude oscillation is typical for the solar wind observations which are dominated by photoelectron pulses. These measurements are only of qualitative value. The sudden decrease in V_{Diff} indicates the onset of the diamagnetic cavity at the IRM spacecraft. Low field values and small photopulses are found in the dense cloud where the conditions are similar to the ionosphere. The modulation is probably due to wake effects. The transition to solar wind after about 19 s is again very sudden and for some seconds modulated by an oscillation with frequency near the lower hybrid frequency $f_{LH} \approx 5$–7 Hz. (Bottom panels: spectrograms) Burst memory ELF/MF electric wave spectrograms measured every 32 ms during release 2. For the frequency scale, see Table 3. The short pulse of $\Delta t \approx 0.7$ s duration coinciding with the decrease in V_{Diff} indicates the passage of the Li cloud boundary and the start of the diamagnetic cavity. After this time, electric wave activity in the cavity is rather quiet for about 4 s. Patchy emissions may indicate the spin-modulated Li plasma frequency. Unstructured noise is present in the transition region from cavity to solar wind. The intense impulsive emission about 17 s after cloud encounter coincides with the region of shocklike transition to the solar wind. This is a shocklike ion beam-excited emission in the ion acoustic wave band. It decays rapidly, but enhanced activity is observed for times much longer than those shown in the picture.

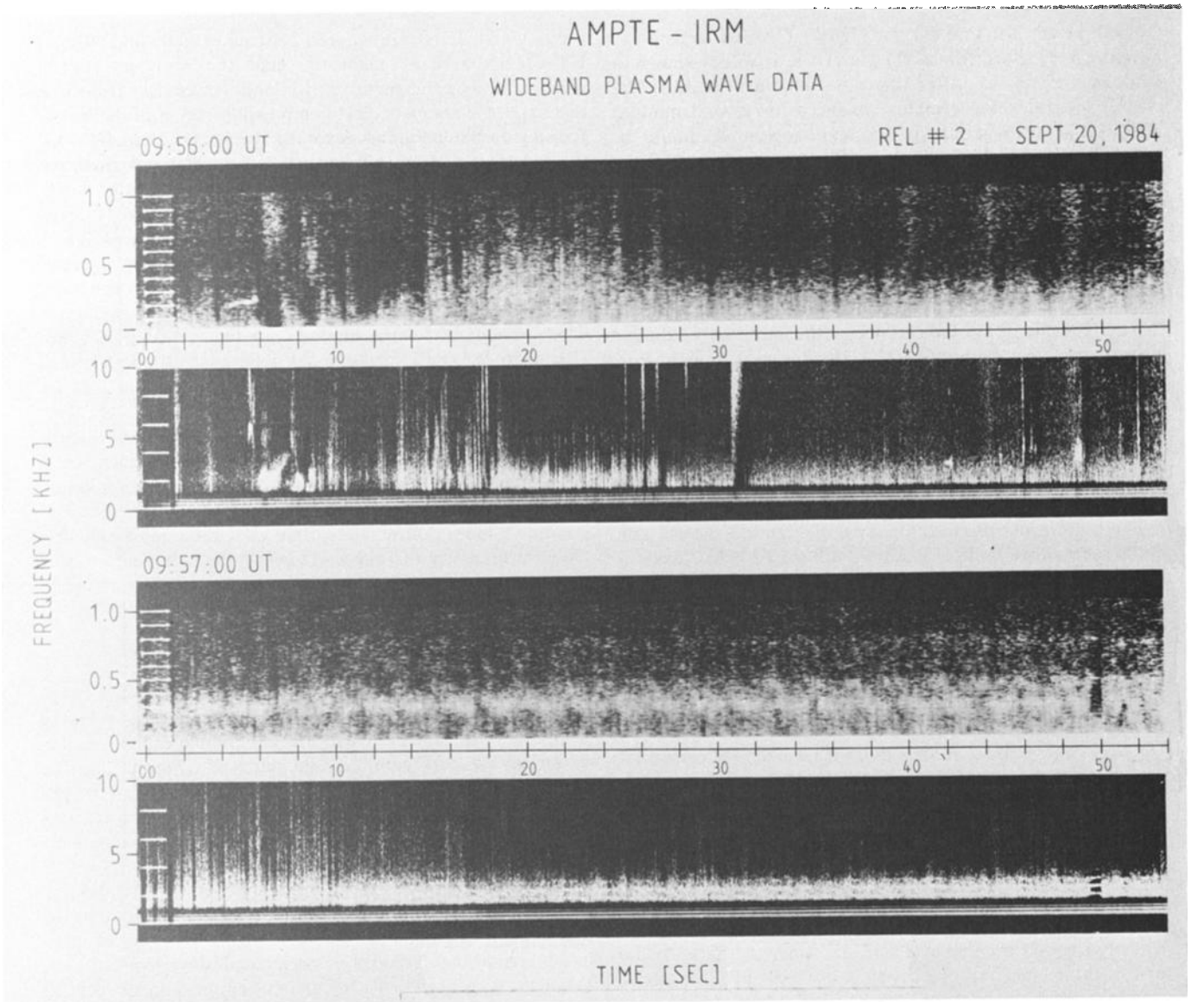

Fig. 4. Wideband plasma wave spectra obtained with the University of Iowa wideband receiver during release 2. Two minutes of observations are shown. The first and third panels from the top give the range 0–1 kHz in high-frequency resolution. The second and fourth panels show the full domain of 1–10 kHz. The release is marked by the sharp pulse above 1 kHz at 0956:01.7 UT. Patchy emissions in the diamagnetic cavity appear above 700 Hz at 0956:07 UT and above 400 Hz at 0956:09 UT. Intense low-frequency noise is seen in relation to the transition region. This noise is highly structured in time at higher frequencies. In the upstream region (after 0957 UT) there appear narrow-band emissions near the electron cyclotron harmonics.

to anomalous diffusion of the solar wind magnetic field into the Li^+ ion cloud. But, as discussed by G. Haerendel (unpublished manuscript, 1985), the emission level is still not high enough to generate the required anomalous diffusion on the time scale of observation.

During release 1 (Figure 2*a*) the qualitative behavior is similar. The wave energy density in the diamagnetic cavity is below the undisturbed solar wind except for the spiky intensification at the first encounter of the cavity with the IRM spacecraft at 0725:04 UT and a pulse after 0725:10 UT. Low energy densities are also found in the early transition region. The values are below those for release 2 for the magnetic field compression region. But the energy density of the intense emission in the shocklike region reaches about the same value as for release 2. In the upstream region the intensity stays on an enhanced level, but the variability is much larger than during release 2. This may be caused by the different magnetic field geometries of the two releases and by differences in the solar wind conditions.

Figure 7 shows a power spectrum of the peak wave emissions between 31 Hz and 178 kHz for the second release at the time of the intense emission in the shocklike region of the transition region (curve 3, 0956:19 UT) compared with typical spectra 1 s before the release (curve 1, 0956:00 UT) and 1 s before (curve 2) and 1 s after (curve 4) the time of the intense shocklike emission. Before the release, spectrum 1 obeys the gradual decay with frequency, having a weak maximum above 100 kHz at the frequencies of the escaping TKR. Spectrum 2 is enhanced at low frequencies right before the maximum of the intense emission. Near the time of maximum intensity, spec-

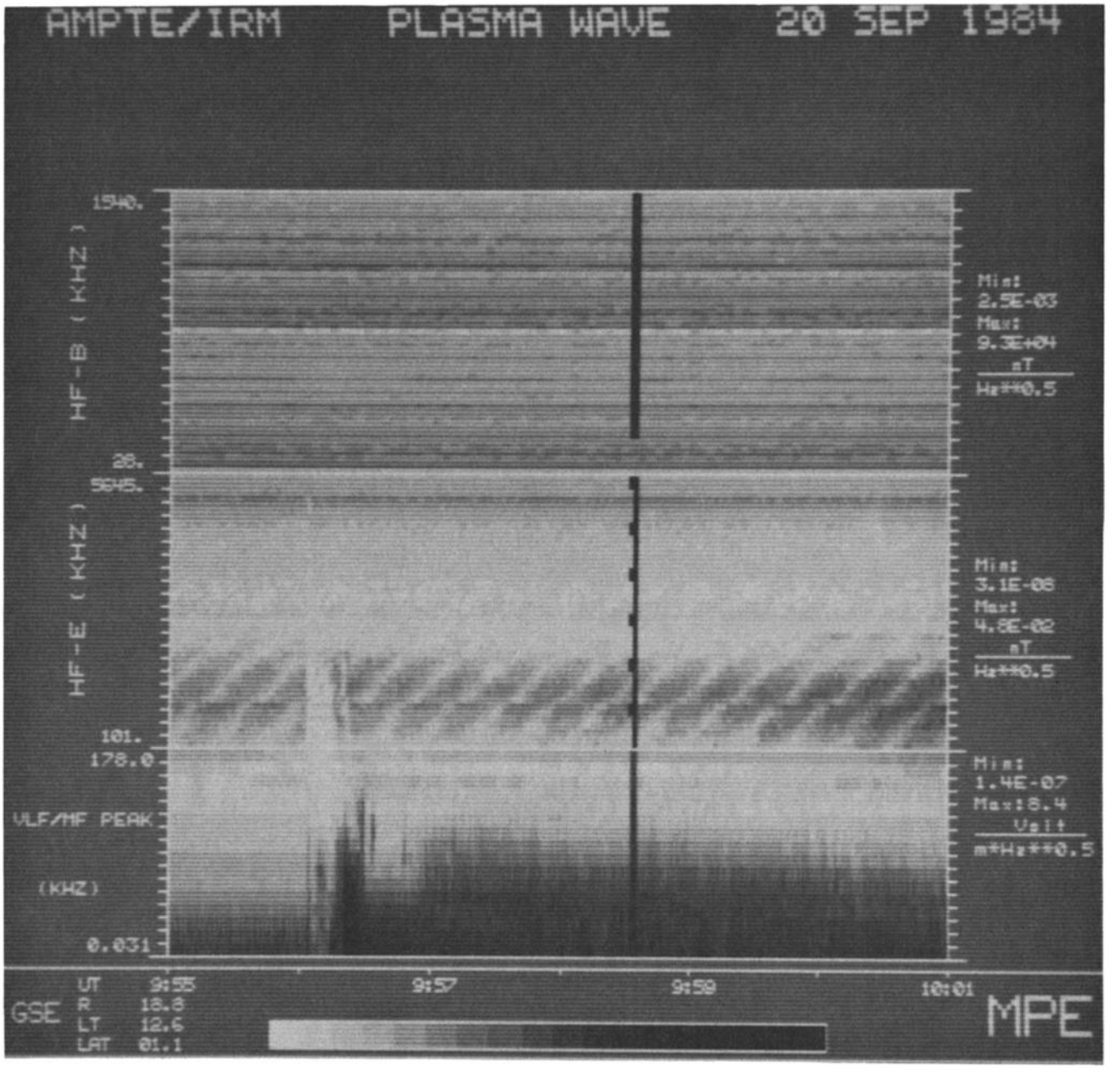

Fig. 5. High-frequency part of the wave spectra for release 2. (Top) Magnetic wave component ranging from 20 kHz to 770 kHz. The presentation is such that each second sweep is shown on top of the first one, separated by the horizontal dashed line. No response is seen in the HF-*B* during the release. (Middle) Electric component covering the range from 101 to 5645 kHz. The frequency scale is divided into 42 channels (two per tip mark); the frequencies are given in Table 2. The emission centered around 300 kHz is the TKR. The higher-frequency background is the GRN. The release attenuates the TKR and GRN around IRM. Return of radiation beginning from high to low frequencies indicates the decrease in plasma density during expansion of the diamagnetic cavity. Inside the cavity, emission at the electron plasma frequency is found at progressively decreasing frequency. (Bottom) The adjacent ELF/MF spectral range as obtained from the peak value measurements. The frequency scale is divided into 16 channels with the corresponding frequencies given in Table 3. Attenuation of radiation and recovery after the density has decreased to low values comparable with the solar wind density is also observed here.

trum 3 has a totally different character. For frequencies below 2 kHz the increase from the preevent level is up to a factor of 10^6 in power spectral density.

The power spectrum of the average wave emission at maximum intensity below 2 kHz (not shown here) decays with frequency approximately as $f^{-3/2}$, while the spectrum of the peak wave emission is about 2 orders of magnitude more intense and has a maximum around 200 Hz. Above 2 kHz it has a sharp cutoff and decays approximately as f^{-7}. In the cutoff region the peak and average power spectra match. At frequencies higher than 17.8 kHz both the average and the peak spectra become flat and slightly enhanced over the undisturbed solar wind.

The intense shocklike emission is very impulsive as seen from the comparison of spectra 2–4. *Gurnett et al.* [this issue] have shown that the spectra at maximum intensity are similar to those measured by ISEE 1 during bow shock crossings [*Gurnett*, 1985]. They conclude that this noise may be an indication of a shocklike interaction between the Li^+ ion cloud and the quickly decelerated solar wind protons.

TABLE 2. HF-*E* Frequencies

Channel	Frequency
1	0.101
2	0.113
3	0.126
4	0.139
5	0.151
6	0.164
7	0.176
8	0.202
9	0.227
10	0.252
11	0.277
12	0.303
13	0.328
14	0.353
15	0.403
16	0.454
17	0.504
18	0.554
19	0.605
20	0.655
21	0.706
22	0.806
23	0.908
24	1.01
25	1.11
26	1.21
27	1.31
28	1.41
29	1.61
30	1.82
31	2.02
32	2.22
33	2.42
34	2.62
35	2.82
36	3.23
37	3.63
38	4.03
39	4.44
40	4.89
41	5.23
42	5.65

Frequencies are in megahertz.

3.6. *Wave Observations With the UKS*

Figure 8 shows a representative sweep of the UKS plasma wave instrument during release 1. The measurement of the spectrum was made with the swept frequency analyzer (SFA), described by *Darbyshire et al.* [1985]. The plasma frequency in the solar wind prior to the release was detected at 9 ± 2 kHz, which is in agreement with the IRM observations (Figure 6*a*). The sharp peaks around 60, 90, and 120 kHz are spacecraft interference lines. The UKS encountered the diamagnetic cavity at 0725:09 UT [*Lühr et al.*, this issue]. At this time the downward frequency sweep had reached a frequency of about 24 kHz. No significant emissions above background noise level can be detected on the sweep until the end of the following two sweeps at 0725:45 UT. During the sweep from 0725:45 to 0726:01 UT, which corresponds to the late phase of the release, the spectrum shows the plasma frequency at 18 kHz with a strongly developed emission. This corresponds to a plasma density of 4 cm^{-3} upstream of the ion cloud, in agreement with the IRM measurements.

The measurements of the correlator aboard UKS were more sensitive, and Figure 9*a* shows the rms wave amplitude between 0.11 and 3.9 kHz measured by the correlator for the time period from 0724:33 to 0726:25 UT during release 1. The correlator was applied to the buffered output of the preamplifier to study the 0- to 4-kHz part of the wave spectrum with a time resolution of 0.5 s [*Darbyshire et al.*, 1985].

At 0725:05–0725:08 UT, before UKS encountered the diamagnetic cavity at 0725:09 UT, the correlator power indicated some wave activity below 4 kHz. The average rms wave amplitude of the corresponding noise was slightly more than 1 mV/m. This activity may already belong to the interaction between the Li^+ ion cloud and the solar wind, because at earlier times the amplitude reached only $\sim 5 \times 10^{-2}$ mV/m (Figure 9*a*). The activity decays to background when the UKS contacts the diamagnetic cavity at 0725:10 UT. Inside the diamagnetic cavity, which is not as clearly defined as in the magnetic measurements of the IRM [*Lühr et al.*, this issue], the power is of a more spiky nature. The wave activity ceases again between 0725:17 and 0725:20 UT, when the UKS magnetic field indicates that the UKS was already outside the cavity. The IRM at this time was in the boundary current region where the wave activity was extremely low. Emission of 1 mV/m amplitude is observed again on UKS at 0725:23 UT in the transition region. Throughout the transition region there is some correlation between the wave intensities recorded simultaneously at 0725:36 UT. But the rms wave amplitude detected by the UKS spacecraft was $E_{rms} = 6$ mV/m, which is only 10% of the $E_{rms} = 50$ mV/m measured on the IRM.

Figure 9*b* presents similar observations for release 2. The wave activity detected by the correlator aboard the UKS was of shorter duration than that for release 1. It was also less intense. The UKS did not encounter the diamagnetic cavity this time, as is obvious from the UKS magnetic field measurements (top panel of Figure 9*b*). Also, the increase of the magnetic field magnitude in the transition region was much flatter on UKS than on IRM, though the field reached about the same compression at the positions of both spacecraft. The UKS wave activity was spiky in nature and low in the region of the gradual increase in B. The wave amplitude is $E_{rms} = 0.7$ mV/m at 0956:10 UT, comparable to the $E_{rms} = 0.6$ mV/m seen at the IRM.

The maximum wave intensity observed on the UKS coincides with passage of the maximum in B at 0956:17 UT, about 4 s before the intense emission detected on the IRM. It reaches a value of $E_{rms} = 2$ mV/m, more than an order of magnitude less than the $E_{rms} = 50$ mV/m in the intense shocklike emission measured by the IRM during this release at 0956:20 UT. Afterward, the wave intensity rapidly decays to the low prerelease value and does not maintain a high and disturbed level as it does on the IRM.

The wave measurements on the UKS and the IRM are thus distinctly different, though certain similarities are obvious in the observations. The differences may, however, be related to the distinctly different behavior of the interaction regions between the solar wind and the Li plasma at the positions of the two spacecraft.

4. DISCUSSION

4.1. *Plasma Density*

The time development of the electron density n_e for the two releases is given in Figure 10. These electron density profiles were obtained from the measurement of the electron plasma frequency inside the Li plasma cloud. As has already been mentioned, the natural emission at the electron plasma frequency was weaker during release 2 than during release 1. However, in the cavity it was also well defined, while the cavity duration was shorter. The questions related to the determination of n_e are discussed by R. R. Anderson et al. (un-

published manuscript, 1985). We have indicated the approximate release times t_0 to the caption to Figure 10. It is obvious that the density in the diamagnetic cavities follows the theoretically predicted slope $n_e \propto (t - t_0)^{-2}$ [*Haerendel et al.*, 1985; G. Haerendel, unpublished manuscript, 1985; R. R. Anderson et al., unpublished manuscript, 1985] for both releases. It should also be noted here that the typical $n \propto t^{-2}$ law for the development of the plasma density is valid only for the time of free expansion of the Li plasma cloud until the largest radius of the diamagnetic cavity is reached. When the IRM crosses the boundary current layer at the beginning of the transition region, the density increases suddenly by about half an order of magnitude, probably owing to a snowplow effect of the plasma cloud in the solar wind, and stays high in the magnetic compression region. In the shocklike region the density decays steeply to the solar wind background density level. It should be noted that this development of the density is different for both releases. Apparent reasons for the differences in time and structure of n_e are the different solar wind conditions. During release 1 the solar wind flow was approximately parallel to the interplanetary magnetic field, while during release 2 the flow and magnetic field were nearly perpendicular to each other. In addition, the flow velocity was much higher during release 1 than during release 2. Moreover, since release 1 took place upstream of but near the bow shock at magnetic field lines which were connected to the bow shock, upstream ion fluxes were present over almost all the observational times. The interaction of these upstream ions also has some effect on the interaction between the Li and solar wind plasmas, at least through the modulation of the interplanetary magnetic field caused by the ion fluxes. Convective plasma losses may be responsible for the steep density decay in the shocklike region of the transition region. The solar wind density itself oscillated by a factor of 2–3 during the releases. This variation masks the further development of the contribution of the Li to the plasma density in the upstream region where the Li plasma density is below the solar wind density.

4.2. *Wave Activity and Quasi-Static Electric Field in the Diamagnetic Cavity*

The ELF/MF wave activity in the diamagnetic cavity starts with a short pulse at the first IRM-cloud encounter. This broadband pulse is probably caused by the diamagnetic drift current instability in the boundary layer. The relevant instability is the modified two-stream instability. For this instability the drift velocity $V_d = |E_\perp/B|$ has to exceed the sound velocity c_s in the boundary layer in order to excite waves in the ion acoustic wave band below the ion plasma frequency f_{Li}. Since the pulse extends up to 10 kHz, this interpretation is consistent with the observation.

Little is known about the electron temperature T_e. If the plasma is dominated by a large number of cold electrons of some 10^3 K temperature, as expected for photoionization of the Li atoms, the plasma instrument will fail to observe these electrons. To some extent this behavior seems to be the case, because the density as measured by the plasma instrument aboard the IRM and inside the diamagnetic cavity is significantly below that determined from the wave experiment [*Paschmann et al.*, this issue]. The threshold of that instrument was about $T_e = 5$ eV, corresponding to $c_s = 8$ km/s. The actual value of c_s may be significantly less than this for $T_e \approx 0.5$ eV. On the other hand, soon after release, heated electrons have been observed with energies up to about the solar wind electron temperature $T_e \approx 30$ eV. In this case, $c_s = 20$ km/s, assuming that the Li^+ ions dominate over the solar wind. For an estimate of the electric field $E_\perp$ in the boundary required to drive the instability, we choose the former value of c_s. Then taking $B \approx 6 - 8$ nT yields $E_\perp \approx 6 \times 10^{-5}$ V/m. Our electric field measurements are not reliable enough to draw a conclusion of the presence of such a field in the initial boundary. However, the required value of $E_\perp$ seems to be reasonable.

In the unmagnetized Li plasma in the diamagnetic cavity we have two types of emissions: the high-frequency electron plasma frequency, which is probably on the level of the thermal plasma fluctuations, and the spiky low-frequency emission below f_{Li}. To check the former assumption, we can calculate the plasma fluctuation level [*Krall and Trivelpiece*, 1973] from $\epsilon_0 E^2/2n_eT_e = (n_e\lambda_D^3)^{-1}$, where λ_D is the Debye length and T_e is measured in electron volts. This estimate yields an average wave energy density ratio of $\lesssim 1.5 \times 10^{-5}$ in the cavity (release 1). Using our density measurements and the temperature as measured by the plasma instrument [*Paschmann et al.*, this issue], we obtain an average rms electric field amplitude $E_{rms} = 3 \times 10^{-4}$ V/m for the electron plasma fluctuations. This amplitude can be compared with the measured intensity at the plasma frequency inside the diamagnetic cavity during release 1. The most reliable measurement was in channel 15 of the high-frequency electric field instrument, when the plasma frequency was at 403 kHz. The power spectral density was about 5×10^{-8} V/m $(\text{Hz})^{1/2}$. Taking into account the 10-kHz bandwidth of the channel, we find an $E_{rms} \approx 0.6 \times 10^{-5}$ V/m well below the above value. This supports the view that the plasma frequency emissions are thermal fluctuations.

The spiky low-frequency emission is in the ion acoustic wave band but has an emission maximum just below f_{Li}. At these low frequencies, waves may be excited by the solar wind proton current flowing across the Li cloud. The relative drift velocity associated with this current is of the order of, or for retarded protons even somewhat less than, the solar wind velocity $V_{sw} < V_e$, which is still much larger than $c_s \approx 8$ km/s. So the current is unstable with respect to ion sound instabilities but stable against the two-stream instability. For these high drift velocities, however, the waves propagate essentially isotropically. The observed spin modulation of the emission just below f_{Li} is, however, unclear, as is the mechanism of its generation. On the basis of conventional theory, the corresponding waves should have short wavelengths ($k^2\lambda_D^2 \sim 1$). The electric antenna would then considerably underestimate the real wave intensity, since the wavelength is shorter than the antenna. Similar observations have been obtained during the Artificial Comet Barium release on AMPTE in December 1984 [*Gurnett et al.*, 1985] and also in later magnetospheric tail release experiments. In all these experiments the heavy ion plasma frequency emission was clearly defined. Its origin is of special interest. This problem will be treated elsewhere.

Another problem is presented by the unsymmetric quasi-static electric field inside the diamagnetic cavity. No anomalous collision frequencies are generated, as is suggested by the low level of wave activity. The Spitzer collision frequency is less than $\nu_e = 3 \times 10^{-3}$ Hz for $T_e \approx 5$ eV. In the most favorable case, when $T_e \approx 0.5$ eV, $\nu_e \approx 1.2$ Hz. Using a measured field of the order of $E \approx 1$ mV/m yields a current density of $j \approx 0.2$ A/m^2, which is far too high. For comparison, the solar wind proton current density in the cloud is only $j_{sw} = en_{sw}v_{sw} \approx 8 \times 10^{-7}$ A/m^2. A possible explanation is that the measured electric field is mainly caused by an interaction of the IRM spacecraft with the ion cloud. It might also be caused by extraction of ions due to the applied solar wind electric field to the cloud. This mechanism is yet barely understood.

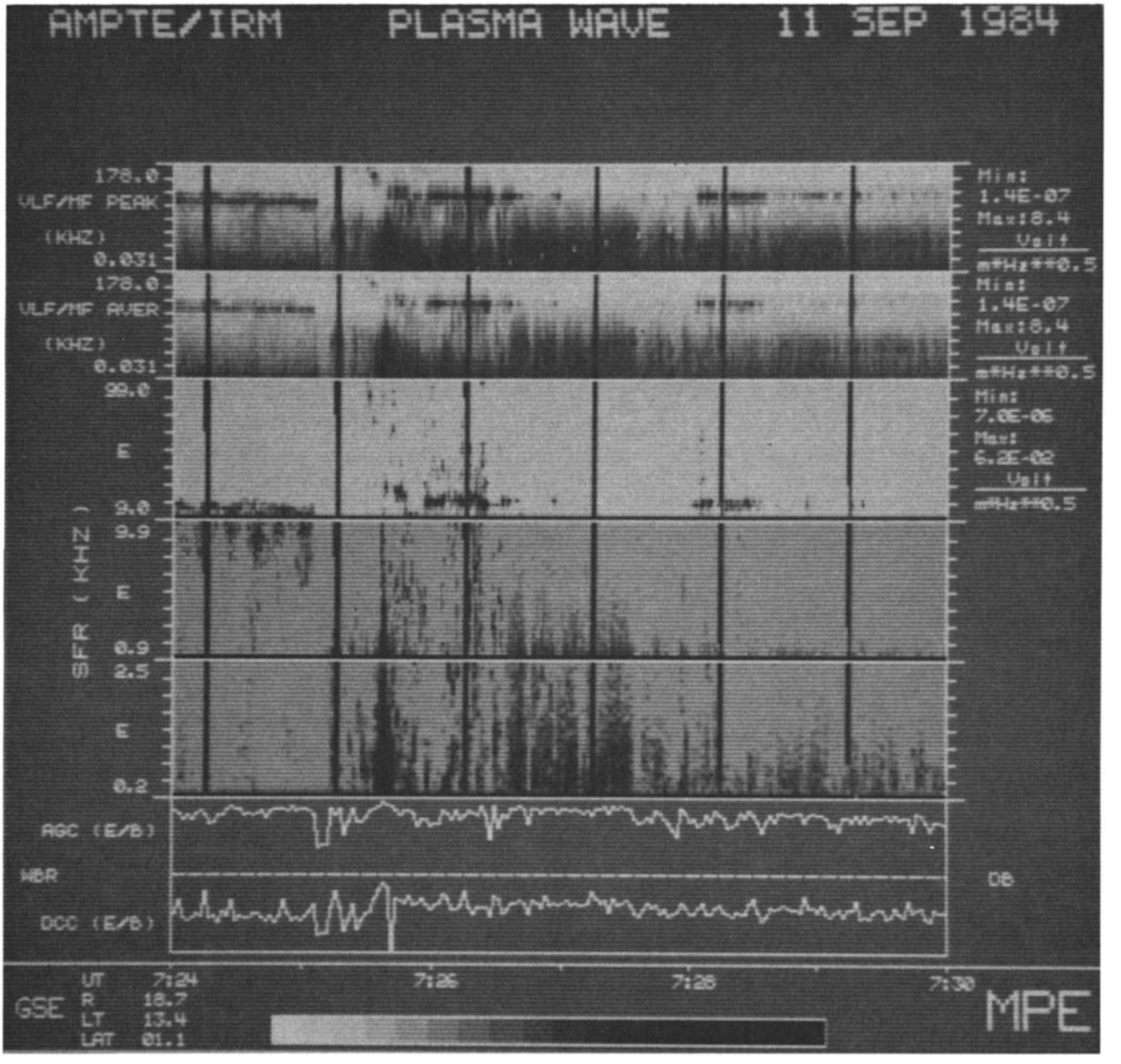

Fig. 6*a*. Prior to release 1 the solar wind electron plasma frequency is seen around 10 kHz in the peak and averages, as is also seen in SFR 3. Dropout of wave activity down to low frequencies coincides with the release. There is, however, some wave activity below 200 Hz in the cavity as seen in the peak. Very intense broadband emission follows at the end of the transition region. Enhanced wave background is found for several minutes after release in the upstream region.

Fig. 6. Spectrograms of ELF/MF waves as obtained with the Iowa plasma wave instrument and the Aerospace/University of Washington stepped frequency receivers (SFR 1–3) for (*a*) release 1 and (*b*) release 2. The presentation is as follows: ELF/MF peak values (top panel), ELF/MF averages (second panel; for the frequency scale, see Table 3), SFR 3–1 (third, fourth, and fifth panels; for the frequency scale, see Table 4), automatic gain control (AGC) and durating current compressor (DCC) signal of wideband data (two bottom panels). During release 2, SFR 1 has been switched to the magnetic antenna. No significant magnetic activity has been found in this channel in connection with the release.

4.3. *Wave Activity in the Transition Region*

In the transition region from the diamagnetic cavity to the solar wind the wave activity rises in both bandwidth and intensity. As is seen in Figure 2, the wave intensity is very low when the steep increase of the magnetic field occurs but rises steeply when the magnetic field is strongly compressed. The low wave level in the steep magnetic field gradient indicates that the boundary between the cavity and the transition region is a fairly stable discontinuity, where both $|\mathbf{B}|$ and n_e experience a sudden jump. An important aspect of these processes is whether or not the wave activity is sufficiently strong to cause enhanced plasma diffusion affecting the momentum balance in the available observation time. A second spacecraft (UKS) positioned apart from the center region of the cloud is extremely useful in answering this question. Previous estimates [*Haerendel*, 1983] suggest that the expected classical diffusion times are too long to make diffusive effects observable on IRM. Within those time scales the solar wind will already

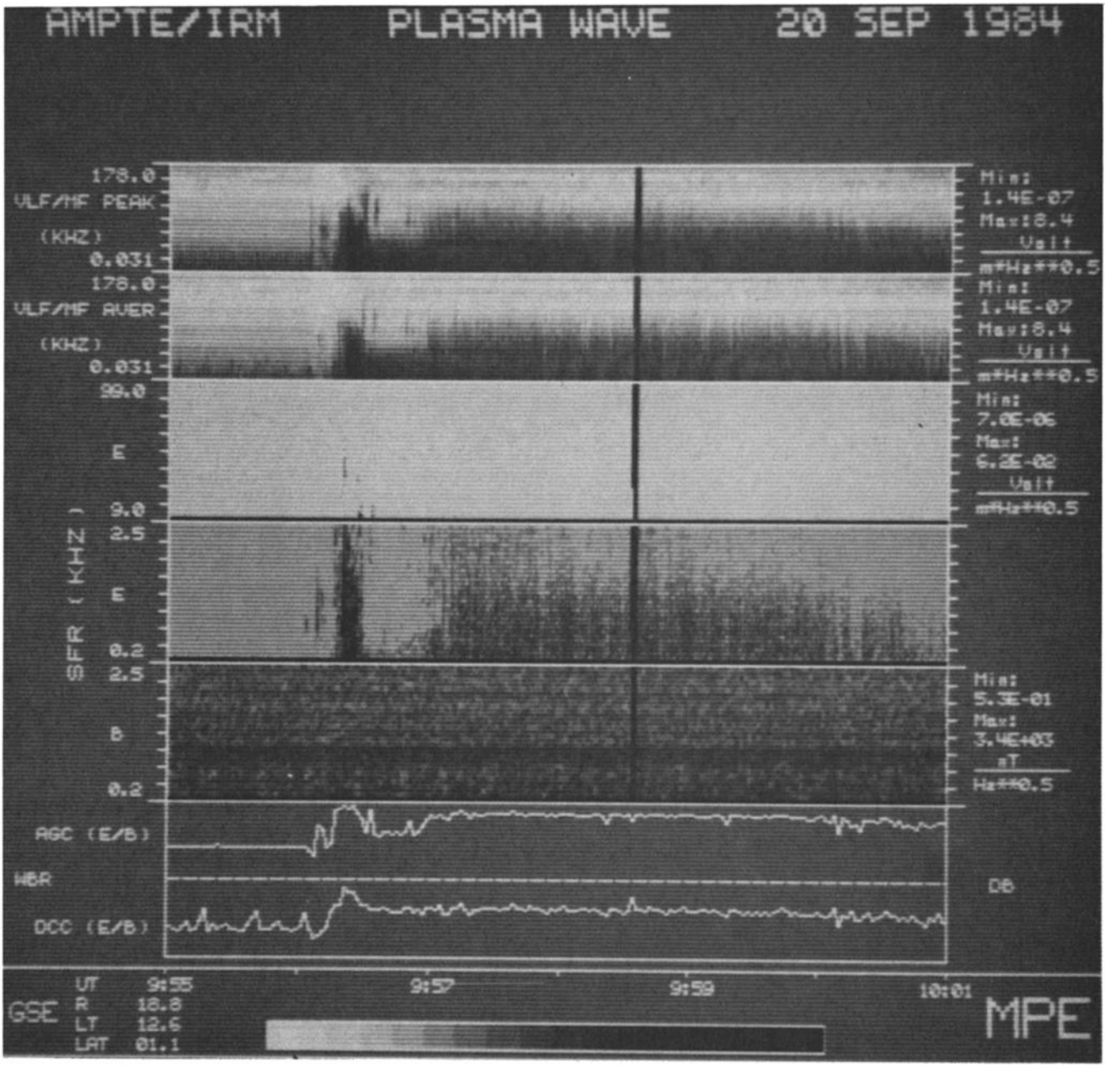

Fig. 6b. Release 2 shows similar but quieter behavior. Most impressive is the short but intense pulse at 0956:20 UT, which is related to the shocklike region of the transition region. In the upstream region, electron cyclotron harmonic waves appear in the peak, average, and SFR. The activity ends about 5–6 min after release.

have transported the cloud far downstream, away from the IRM position. However, this time interval could be shortened considerably by anomalous diffusion due to wave excitation. If this is the case, diffusive effects could be observable. It is, however, an important result of these measurements that the wave intensity observed in the transition region is too low by orders of magnitude to cause any anomalous diffusion, at least over the times of the in situ observations (G. Haerendel, unpublished manuscript, 1985). In the transition region the spectrum is unstructured and is below the local ion plasma frequency f_{Li}. These waves are believed to propagate in the ion acoustic wave mode, although higher harmonic electrostatic ion cyclotron waves may also be present. The proton cyclotron frequency is about 0.6 Hz, so that ion cyclotron waves would not be resolved by the plasma wave instruments. The electron cyclotron frequency is $f_{ce} \approx 1.1$ kHz. There is, however, no indication of any emissions in the whistler mode, since no magnetic wave fields were detected during release 2.

The quasi-static electric field in the magnetic compression region is low (Figure 3). It experiences a sudden change in character at the end of the compression region approximately at the time when the very intense low-frequency [*Gurnett et al.*, this issue] emission sets in. This relationship is suggested by a comparison of the shock memory and quasi-static electric field measurements (Figure 3). Afterward, the quasi-static electric potential remains, however, modulated for a time of about 6 s. This modulation can be divided roughly into a low- and a high-frequency modulation. The high-frequency part has a frequency of a few hertz, typically about 5–7 Hz. This frequency is near the lower hybrid frequency in a 10-nT field ($f_{LH} \approx 6.5$ Hz). This modulation may thus be caused by lower hybrid waves present upstream of but adjacent to the Li cloud. Both

TABLE 3. ELF/MF Frequencies

Channel	Frequency
1	0.031
2	0.056
3	0.100
4	0.178
5	0.311
6	0.562
7	1.000
8	1.780
9	3.11
10	5.62
11	10.00
12	17.80
13	31.10
14	56.20
15	100.00
16	178.00

Frequencies are in kilohertz.

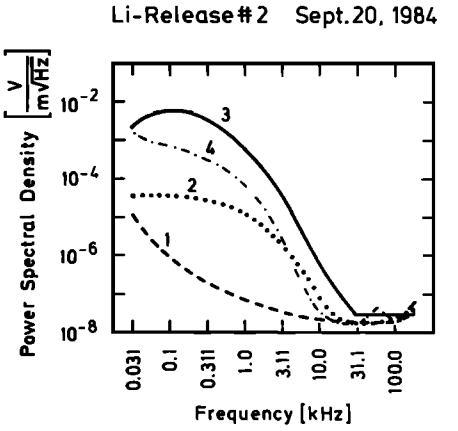

Fig. 7. Power spectrum of ELF/MF emission for release 2 at the time of the shocklike emission. For comparison, the prerelease solar wind power spectrum is shown. The spectrum has a maximum at low frequencies and decays steeply at high frequencies greater than 30 kHz. The power is increased by orders of magnitude above undisturbed solar wind power. Curves 2 and 4 show spectra 1 s before and 1 s after maximum emission, respectively.

the intense plasma wave emission and the lower hybrid waves are often related to a shock transition [*Gurnett*, 1985]. The lower hybrid waves may be driven by the density gradient via the lower hybrid drift instability, while the intense emission at the transition to solar wind is probably driven by an ion-ion beam interaction [*Gurnett et al.*, this issue].

4.4. *Waves at the Position of the UKS Subsatellite*

As indicated by the magnetic field observations on the UKS subsatellite (cf. Figure 9), the UKS never was deep inside the diamagnetic cavity [*Lühr et al.*, this issue]. The releases were symmetrical with respect to the position of the IRM spacecraft. The UKS was positioned upstream but sideways of the IRM. During release 1 it felt a short magnetic field depression during the time that the IRM was in the diamagnetic cavity. This suggests that the UKS just touched the boundary of the cavity. G. Haerendel (unpublished manuscript, 1985) estimates that the cavity might just have have reached the UKS for the conditions of release 1 when the maximum cavity radius was about 35 km. During release 2 the UKS was clearly outside the cavity. It never observed a depression in the magnetic field but slowly entered the transition region. The IRM, in contrast, crossed all three physically interesting regions: the diamagnetic cavity, the transition region, and the upstream region. It is thus quite natural to expect that the wave activities observed on both spacecraft may be different. Nevertheless, there is some striking similarity in the wave intensities measured on UKS and IRM, as is obvious from Figure 9. First, note that enhanced wave activity was observed on the UKS during both releases. During release 1 it started 5 s before the UKS contacted the diamagnetic cavity. The electrostatic wave amplitudes were about 1.5 mV/m. At this time the cavity was already well developed at the position of the IRM. So the UKS at its upstream position received information, transported by the waves, of the existence of the cavity in advance, while in the magnetic field there was no indication of the cavity yet. When touching the cavity the UKS wave activity was still enhanced ($\approx$1 mV/m) but highly variable. After the UKS left the cavity, there was a clear correlation between the measurements of the wave intensity on the IRM and the UKS. In particular, during release 1 both spacecraft observed the intense emission in the shocklike region of the transition region at the same time (0725:35–0725:36 UT). The intensities of this emission are, however, different on both spacecraft. In general, UKS observes smaller rms electric field amplitudes. This might, of course, be an artifact, because the UKS instrument excludes the frequency range below 110 Hz. This could cause a difference of a factor of roughly 2 in E_{rms}. In addition, the UKS antenna was much shorter than the IRM antenna, so that the shorter and less intense wavelengths may give the main contribution to the UKS wave intensity.

From these facts we conclude that during release 1 the tran-

TABLE 4. SFR Frequencies

Channel	SFR 1	SFR 2	SFR 3
1	CAL	CAL	CAL
2	0.275	0.900	9.00
3	0.350	1.200	12.00
4	0.425	1.500	15.00
5	0.500	1.800	18.00
6	0.575	2.100	21.00
7	0.650	2.400	24.00
8	0.725	2.700	27.00
9	0.800	3.000	30.00
10	0.875	3.300	33.00
11	0.950	3.600	36.00
12	1.025	3.900	39.00
13	1.100	4.200	42.00
14	1.175	4.500	45.00
15	1.250	4.800	48.00
16	1.325	5.100	51.00
17	1.400	5.400	54.00
18	1.475	5.700	57.00
19	1.550	6.000	60.00
20	1.625	6.300	63.00
21	1.700	6.600	66.00
22	1.775	6.900	69.00
23	1.850	7.200	72.00
24	1.925	7.500	75.00
25	2.000	7.800	78.00
26	2.075	8.100	81.00
27	2.150	8.400	84.00
28	2.225	8.700	87.00
29	2.300	9.000	90.00
30	2.375	9.300	93.00
31	2.450	9.600	96.00
32	2.525	9.900	99.00

Frequencies are in kilohertz. CAL is calibration.

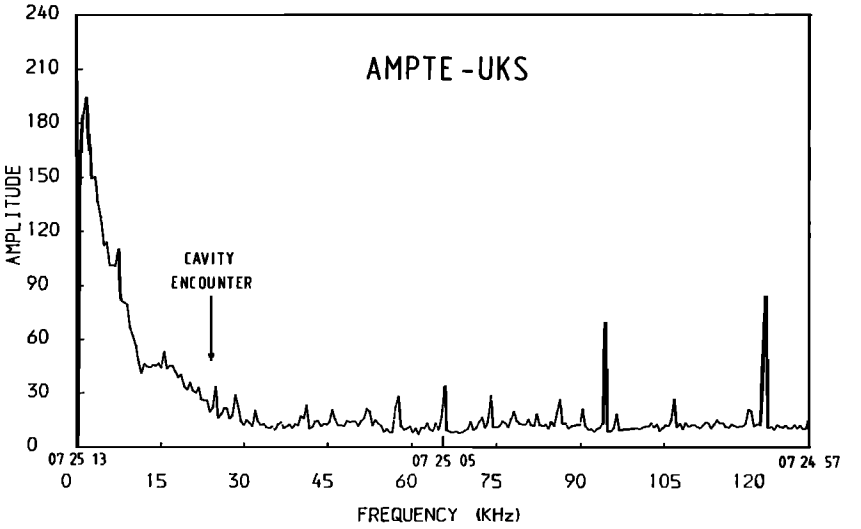

Fig. 8. Spectrum of plasma waves as measured by the UKS for release 1. The 16-s sweep of the receiver is shown. The full range (256) corresponds to a dynamic amplitude of 60 dB. The maximum amplitude 256 corresponds to 3.2×10^{-5} V/m $Hz^{1/2}$. The instrument was operated in a downward frequency stepped mode.

sition region at the positions of UKS and IRM varied similarly. In particular, the shocklike region, where the density drops to solar wind level [*Gurnett et al.*, this issue; R. R. Anderson et al., unpublished manuscript, 1985] has been crossed simultaneously by both spacecraft.

The situation was different for release 2. No direct correlations between the UKS and the IRM measurements were found. The event was much shorter on the UKS than on the IRM. Moreover, contrary to release 1, the shocklike intense emission was not seen simultaneously on both spacecraft. The latter observation indicates that the shocklike transition from the transition region to the upstream region occurred earlier on the UKS than on the IRM. UKS at its upstream position may have left the transition region earlier during release 2 than did IRM.

4.5. *Differences Between the Releases*

In general, there are more similarities than differences between releases 1 and 2. The few differences can probably be traced back to the different interplanetary conditions (G. Haerendel et al., unpublished manuscript, 1985, and G. Haerendel, unpublished manuscript, 1985). The most striking difference was the shorter duration of the solar wind disturbance caused by the Li cloud during release 2, as can be seen from a comparison of the densities (Figure 10) determined from the electron plasma frequency. Also, the onset of the very intense shocklike electrostatic emission was not as sudden during release 1 but was more gradual than during release 2. It is of interest to mention that the intensity of the shocklike emission reached the same value for both releases at the posi-

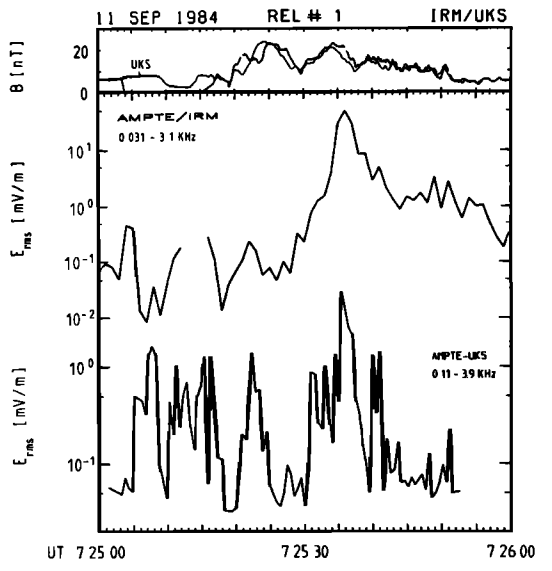

Fig. 9*a*. Release 1.

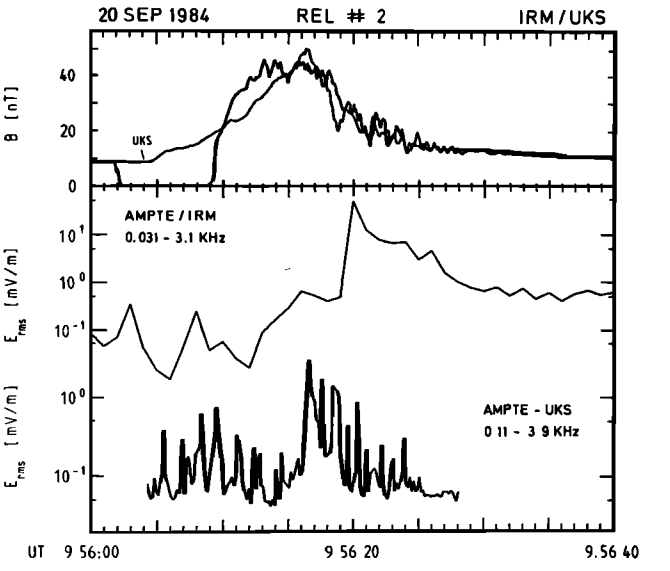

Fig. 9*b*. Release 2.

Fig. 9. Root-mean-square (rms) electric field amplitudes below 3.9 kHz, as measured by the UKS plasma wave correlator, compared with the rms electric field of the IRM ELF/MF plasma wave instrument below 3.1 kHz. For reference the magnitude of the magnetic field as measured by the IRM and the UKS spacecraft is drawn in the top panels.

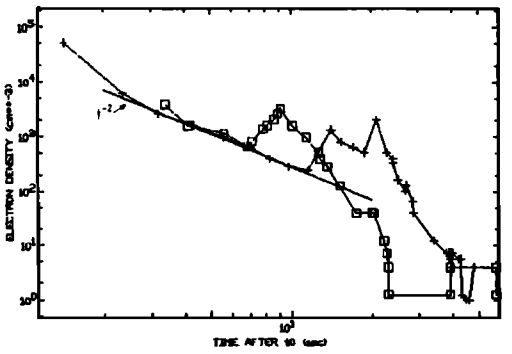

Fig. 10. Time development of the plasma density (after release time t_0) determined from the electron plasma frequency. Release 1 (crosses): t_0 = 0725:03.2 UT. Release 2 (squares): t_0 = 0956:01.6 UT. In the diamagnetic cavity the density follows closely the theoretical slope $(t - t_0)^{-2}$ of the tangential line. The boundary of the Li plasma cloud is characterized by a dense shell. Outside this shell the density decreases steeply to solar wind level. The differences between the two releases are caused by different ambient release conditions.

tions of the two spacecraft. The excitation mechanism therefore seems to be rather insensitive to changes in the environmental conditions. Finally, though the solar wind disturbance lasted longer for release 1, the duration of the wave activity was similar for both releases, of the order of several minutes. However, while this activity was comparably quiet during release 2, it was much more disturbed and spiky during release 1. As a consequence, during release 1 the electron cyclotron waves were not as evident as during release 2.

The reason for these differences is probably due to the different magnetic field and flow conditions. The stronger disturbance of B during release 1 causes a modulation of the wave activity. In addition, release 1 was strongly disturbed by upstream ion fluxes [*Paschmann et al.*, this issue; G. Haerendel, unpublished manuscript, 1985; G. Haerendel et al., unpublished manuscript, 1985]. It is well known that such fluxes generate disturbances in the magnetic field via streaming instabilities. Also, direct interaction of the upstream ions with either the Li plasma cloud or newly born Li^+ ions via the ion-ion beam interaction will contribute to changes in wave activity. The investigation of the related questions is outside the scope of the present overview. It is left for special future investigations.

5. SUMMARY

A variety of plasma wave excitations have been measured during the two Li releases in the solar wind upstream of the earth's bow shock wave. The appearance of these emissions can be related to the different phases of the Li cloud development and the different spatial regimes of the Li plasma–solar wind interaction. These regions are (1) the diamagnetic cavity, (2) the transition region from the diamagnetic cavity to the solar wind, and (3) the upstream region where the solar wind is still influenced by the presence of Li^+ ions. These are rough subdivisions. The diamagnetic cavity on IRM starts with the passage over the spacecraft of a thin front. Also, the transition region consists of the boundary current layer adjacent to the cavity, the magnetic field compression region, and the shocklike transition region from magnetic field and density compression to the solar wind. The observations indicate that the general features of the interaction between the Li plasma and the solar wind are very well reproduced from release 1 to release 2 . In summary, the passage of the front is marked by a short broadband electrostatic pulse with frequencies below the Li^+ ion plasma frequency. In the region of the diamagnetic cavity, waves near the electron and Li^+ ion plasma frequencies are excited. The emission near the electron plasma frequency is at the thermal plasma fluctuation level. Otherwise, the wave activity decreases below the level of the undisturbed solar wind. The reduced wave activities are due to the exclusion of a number of instabilities in the cloud (such as heat flux instabilities which work in the magnetized solar wind). It is most important that in the sharp boundary current layer between the diamagnetic cavity and the magnetic field compression region the wave activity is extremely low. In spite of the strong currents that must necessarily flow in this region, the boundary is thus stable against current instabilities, at least over the time of observation. This finding also excludes any magnetic field diffusion for the time of the in situ measurements. Increasing wave activity is found throughout the magnetic compression region. The corresponding wave emissions are correlated with the magnetic field in both intensity and upper cutoff frequency. In the upstream region, long-lasting continuous emission of electrostatic plasma waves in the ion sound and electron cyclotron wave bands is detected. These waves can be excited by electron temperature anisotropies and electron heat flux but may also be a result of the locally born and accelerated Li^+ ions.

Three striking effects were observed. The first is the attenuation of external high-frequency electromagnetic radiation by the dense Li plasma in the diamagnetic cavity. This attenuation can be understood as a reflection of the radiation at the local plasma frequency (R. R. Anderson et al., unpublished manuscript, 1985).

The second is the almost total dropout of the quasi-static electric field and low-frequency electrostatic wave activity inside the diamagnetic cavity. This dropout of the field can be understood quite naturally as the impossibility for an electrostatic field to exist in the collision-free unmagnetized plasma confined in the diamagnetic cavity. The quasi-static field reappears suddenly in coincidence with the shocklike region. In a similar way, inside the diamagnetic cavity there are no sources of free energy to drive any strong instabilities in the two possible wave modes, the ion acoustic wave and the electron plasma wave. The electron plasma frequency observed has been found to be on the thermal fluctuation level. The weak ion acoustic noise detected in the cavity may be caused by decelerated solar wind protons traversing the cavity. There is still no satisfactory explanation for the weak emissions which may have been detected in the vicinity of the Li^+ ion plasma frequency. Most probably, they are excited by a very slow ion beam.

The third effect is the intense burst of low-frequency plasma waves occurring in the shocklike transition region. This burst may be excited by an ion beam instability related to the transition from the dominating Li^+ to the dominating solar wind plasma [*Gurnett et al.*, 1985, this issue]. It coincides with the decay in the plasma density to the solar wind level where both the solar wind and the Li plasma are of about the same densities. This may be the region where the solar wind protons experience strongest deceleration. It also coincides with the recovery of the quasi-static electric field which is an indication of the transition to the solar wind regime. This emission is seen on both spacecraft though not necessarily at the same time. It is of interest that there is an indication of the presence of lower hybrid waves in the upstream region adjacent to the shocklike region. Its generation, and also the extent to which the presence of the pick-up Li^+ ion beam established from the

plasma data [*Paschmann et al.*, this issue; *Coates et al.*, this issue] contributes to the wave excitations, will be problems to be discussed in future work. Some of the questions listed are the subject of other papers in this issue.

Acknowledgments. We wish to express our thanks to all our colleagues whose efforts made this experiment a successful one. In particular, we acknowledge the technical support by K. Gnaiger (Kurt-Gnaiger-Mikroelektronik, Garching, Federal Republic of Germany), F. Eberl (MPE), D. Odem (University of Iowa), and W. B. Harbridge (The Aerospace Corporation). We have benefited from discussions with G. Paschmann, M. Scholer, I. Papamastorakis, W. Baumjohann, and A. Valenzuela. H. Höfner's contribution to the computational work in data reduction is thankfully acknowledged. The UKS experimenters acknowledge the efforts of E. J. Gershung (University of Sussex), D. Jones and H. Gough (British Antarctic Survey), J. A. Thompson, G. A. Whitehurst, and G. A. Wilson (University of Sheffield). D. J. Southwood (Imperial College, London) is acknowledged for the use of the UKS magnetometer data. The research at the University of Iowa was supported by the Office of Naval Research contracts N00014-82-K-0183 and N00014-76-C-0016 and by NASA grants NGL-16-001-002 and NGL-16-001-043. The research at The Aerospace Corporation was supported in part by the Office of Naval Research and in part by the U.S. Air Force System Command's Space Division under contract F04701-84-C0085. The research at the University of Washington was supported by the Office of Naval Research under contract N00014-84-K-0160. The UKS experimenters were supported by research grants from the U.K. Science and Engineering Research Council. Research at the Technische Universität Braunschweig has been supported by a grant from the Bundesministerium für Forschung und Technologie.

The Editor thanks R. Gendrin and R. L. Tokar for their assistance in evaluating this paper.

REFERENCES

Acuña, M. H., G. W. Ousley, R. W. McEntire, D. A. Bryant, and G. Paschmann, AMPTE—Mission overview, *IEEE Trans. Geosci. Remote Sens.*, *GE-23*, 175, 1985.

Ashour-Abdalla, M., and C. F. Kennel, VLF electrostatic waves in the magnetosphere, in *Physics of the Hot Plasma in the Magnetosphere*, edited by B. Hultqvist and L. Stenflo, p. 201, Plenum, New York, 1975.

Brown, L. W., The galactic radio spectrum between 130 kHz and 2600 kHz, *Astrophys. J.*, *180*, 359, 1973.

Coates, A. J., A. D. Johnstone, M. F. Smith, and D. J. Rodgers, AMPTE-UKS ion experiment observations of lithium releases in the solar wind, *J. Geophys. Res.*, this issue.

Darbyshire, A. G., E. J. Gershung, S. R. Jones, A. J. Norris, J. A. Thompson, G. A. Whitehurst, G. A. Wilson, and L. Woolliscroft, The UKS wave experiment, *IEEE Trans. Geosci. Remote Sens.*, *GE-23*, 311, 1985.

Dassoulas, J., D. Margolies, and M. Peterson, The AMPTE-CCE spacecraft, *IEEE Trans. Geosci. Remote Sens.*, *GE-23*, 182, 1985.

Gurnett, D. A., The earth as a radio source: Terrestrial kilometric radiation, *J. Geophys. Res.*, *79*, 4227, 1974.

Gurnett, D. A., The earth as a radio source: The nonthermal continuum, *J. Geophys. Res.*, *80*, 2751, 1975.

Gurnett, D. A., Plasma waves and instabilities, in *Collisionless Shocks in the Heliosphere: Reviews of Current Research, Geophys. Monogr. Ser.*, vol. 35, edited by B. T. Tsurutani and R. G. Stone, pp. 207–224, AGU, Washington, D. C., 1985.

Gurnett, D. A., R. R. Anderson, O. H. Bauer, G. Haerendel, B. Häusler, R. A. Treumann, H. C. Koons, and R. H. Holzworth, Plasma waves associated with the AMPTE artificial comet, *Science*, in press, 1985.

Gurnett, D. A., T. Z. Ma, R. R. Anderson, O. H. Bauer, G. Haerendel, B. Häusler, G. Paschmann, R. A. Treumann, H. C. Koons, R. H. Holzworth, and H. Lühr, Analysis and interpretation of the shock-like electrostatic noise observed during the AMPTE solar wind lithium releases, *J. Geophys. Res.*, this issue.

Haerendel, G., Plasma confinement and interaction experiments, Active Experiments in Space, Proceedings of an International Symposium Held in Alpbach, Austria, 24–28 May, 1983, *Eur. Space Agency Spec. Publ.*, *ESA-SP 195*, 337, 1983.

Haerendel, G., et al., The Li/Ba release experiments of the ion release module, *IEEE Trans. Geosci. Remote Sens.*, *GE-23*, 253, 1985.

Häusler, B., F. Melzner, J. Stöcker, P. Parigger, K. Sigritz, R. Schöning, E. Seidenschwang, F. Eberl, B. Merz, U. Pagel, E. Wiezorrek, and R. Genzel, The AMPTE-IRM satellite, *IEEE Trans. Geosci. Remote Sens.*, *GE-23*, 192, 1985*a*.

Häusler, B., R. R. Anderson, D. A. Gurnett, H. C. Koons, R. H. Holzworth, O. H. Bauer, R. A. Treumann, K. Gnaiger, D. Odem, W. B. Harbridge, and F. Eberl, The plasma wave instrument onboard the AMPTE-IRM satellite, *IEEE Trans. Geosci. Remote Sens.*, *GE-23*, 267, 1985*b*.

Krall, N. A., and A. W. Trivelpiece, *Principles of Plasma Physics*, p. 567, McGraw-Hill, New York, 1973.

Lühr, H., D. J. Southwood, N. Klöcker, M. Acuña, B. Häusler, M. W. Dunlop, W. A. C. Mier-Jędrzejowicz, R. P. Rijnbeek, and M. Six, In situ magnetic field measurements during AMPTE solar wind Li^+ releases, *J. Geophys. Res.*, this issue.

Paschmann, G., C. W. Carlson, W. Baumjohann, H. Loidl, D. W. Curtis, N. Sckopke, and G. Haerendel, Plasma observations on AMPTE/IRM during the lithium releases in the solar wind, *J. Geophys. Res.*, this issue.

Pilipp, W. E., Expansion of an ion cloud in the earth's magnetic field, *Planet. Space Sci.*, *19*, 1095, 1971.

Scholer, M., On the motion of artificial ion clouds in the magnetosphere, *Planet. Space Sci.*, *18*, 977, 1970.

Ward, A. K., D. A. Bryant, T. Edwards, D. J. Parker, A. O'Hea, T. J. Patrick, P. H. Sheather, K. P. Barnsdale, and A. M. Cruise, AMPTE/UKS spacecraft, *IEEE Trans. Geosci. Remote Sens.*, *GE-23*, 202, 1985.

R. R. Anderson and D. A. Gurnett, Department of Physics and Astronomy, University of Iowa, Iowa City, IA 52242.

O. H. Bauer, G. Haerendel, B. Häusler, and R. A. Treumann, Max-Planck-Institut für Physik und Astrophysik, Institut für extraterrestrische Physik, 8046 Garching, Federal Republic of Germany.

P. J. Christiansen, M. P. Gough, and A. J. Norris, University of Sussex, Falmers, Brighton, Sussex BN 19QH, England.

A. G. Darbyshire, S. R. Jones, and L. J. Woolliscroft, Physics Department, University of Sheffield, Sheffield S3 7RH, England.

R. H. Holzworth, Geophysics Program, University of Washington, Seattle, WA 98195.

N. Klöcker and H. Lühr, Institut für Geophysik und Meteorologie, Technische Universität Braunschweig, 33 Braunschweig, Federal Republic of Germany.

H. C. Koons, The Aerospace Corporation, P. O. Box 92957, Los Angeles, CA 90009.

(Received April 22, 1985;
revised September 11, 1985;
accepted September 12, 1985.)